

# Automatic Optimization of Multichannel Electrode Configurations for Robust Fetal Heart Rate Detection by Blind Source Separation

Alessandra Galli , Member, IEEE, Elisabetta Peri , Chiara Rabotti , Sotir Ouzounov ,  
and Massimo Mischi , Senior Member, IEEE

## I. INTRODUCTION

**Abstract—Objective.** Fetal heart rate (fHR) evaluation is fundamental to guarantee timely medical intervention in case of pregnancy complications. Due to the limitations of traditional cardiotocography, multichannel electrophysiological recording was proposed as a viable alternative, which requires Blind Source Separation (BSS) techniques. Yet effective and reliable separation of the fetal ECG remains challenging due to multiple noise sources and the effects of varying fetal position. In this work, we demonstrate that the adopted electrode configuration plays a key role in the effectiveness of BSS and propose guidelines for optimal electrode positioning. Moreover, a model is proposed to automatically predict the most suited configuration for accurate BSS-based fHR estimation with a minimal number of leads, to facilitate practical implementation. **Methods.** We compared fHR estimation accuracy with different electrode configurations on *in-silico* data, identifying the optimal configuration for a recent BSS method. Based on features extracted from raw signals, we proposed a support vector regression model to automatically identify the best electrode configuration in terms of fHR estimation accuracy and to dynamically adjust it to varying fetal presentation. Evaluation was performed on real and synthetic data. **Results.** Guidelines for the optimal electrode configuration are proposed by using 4 leads. Prediction of configuration quality shows 80.9% accuracy; the optimal configuration is recognized in 92.2% of the subjects. **Conclusion.** The proposed method successfully predicts the quality of the configurations, demonstrating the impact of the electrode configuration on the BSS performance. **Significance.** The method holds potential for long-term fetal monitoring, by dynamically choosing the optimal configuration.

**Index Terms—**Automatic quality assessment, blind source separation, electrode configuration, electrode placement, fetal heart rate, fetal position, multi-channel measurements, prediction, support vector regression.

Manuscript received 10 May 2022; revised 4 September 2022; accepted 30 September 2022. Date of publication 6 October 2022; date of current version 21 March 2023. This work was supported in part by the Dutch Research Council (NWO) under Grant HTSM 14663 (EWAM). (Corresponding author: Alessandra Galli.)

Alessandra Galli is with the Department of Information Engineering, University of Padua, 35122 Padua, Italy (e-mail: alessandra.galli@unipd.it).

Elisabetta Peri and Massimo Mischi are with the Department of Electrical Engineering, Eindhoven University of Technology, The Netherlands.

Chiara Rabotti and Sotir Ouzounov are with the Philips Research, Eindhoven, The Netherlands.

Digital Object Identifier 10.1109/TBME.2022.3212587

NOWADAYS, about 20% of pregnancies are complicated [1]. The fetal heart rate (fHR) is considered one of the most important parameters for assessment of the fetal condition during pregnancy and delivery, enabling early detection of complications and subsequent timely intervention. However, current monitoring techniques preclude long-term monitoring of fetal well-being throughout pregnancy. Typically, fetal monitoring during pregnancy is performed by cardiotocography (CTG), which uses Doppler ultrasound to determine the fHR [2]. Doppler ultrasound measurements are unsuitable for long-term, extramural monitoring, since they need frequent repositioning of the ultrasound probe by specialized staff to overcome signal loss [3].

Despite some limitations due to the formation of the vernix caseosa, an electrically isolating layer surrounding the fetus, fetal electrocardiography (fECG) has been introduced as a valid alternative to overcome the CTG limitations [4], [5]. The fECG signal can be non-invasively acquired with electrodes positioned on the maternal abdomen. However, the signals acquired by the electrodes are a mixture of components such as the fECG, which is the one of interest, and others, such as the maternal ECG (mECG) signal, the abdominal electromyogram (EMG), the electrohysterogram (EHG), motion artifacts, and power-line interference. In order to detect the fHR, identification and isolation of the components corresponding to the electrical activity of the fetal heart is needed. The most suitable and widely employed approaches for this type of problem are based on Blind Source Separation (BSS) techniques, which are considered the most promising in terms of robustness and performance for fHR detection [6]. They exploit the spatial correlation of multi-channel recordings to separate the source signals from a set of mixed signals by assuming the mixing is linear and stationary [7]. The signal characteristics are influenced by the spatial position where the signals are acquired; therefore, one of the critical issues of fECG is the choice of the electrode configuration, i.e., the selection of electrode number, position and the choice of the leads. Indeed, the electrode configuration has a crucial influence on the quality of the electrophysiological signals, as it can result in enhanced features of interest [8] or, on the contrary, it may enhance artifacts and reduce the sensitivity to fECG abnormalities [9]. The position of the fetus should also be considered when

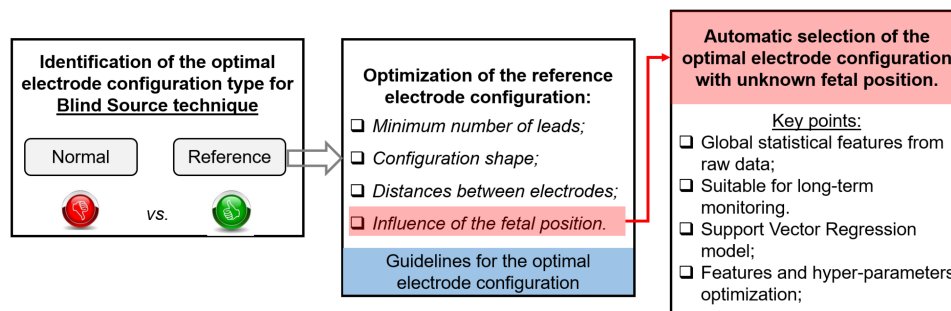


Fig. 1. Scheme of the main contributions proposed by this work.

defining the electrode configuration [10]. Indeed, the position of the fetus affects the pathways along which the biopotentials in the fetal heart are conducted to the abdominal surface [11]. Accurate determination of the fetal position requires ultrasound imaging.

A further requirement for electrode configurations in long-term monitoring is to minimize the number of electrodes, to increase patient comfort and ease the positioning procedure. Less electrodes are also associated with reduced electronics and power consumption for signal conditioning [12].

In the literature, numerous electrode configurations have been proposed to enhance the fECG signal quality, which is commonly assessed by the signal-to-noise ratio (SNR) [13]. For instance, in [8] the influence of the electrode positions of six bipolar leads on the SNR is investigated in the last phases of pregnancy, demonstrating a significant influence of bipolar lead orientation and inter-electrode distance on maternal and fetal ECG measurement quality. The setup selected in [14] consists of five bipolar leads and reduces common mode signals, resulting in the attenuation of the contribution of the mECG to the recordings and the enhancement of the relative contribution of the fECG. As a result, the SNR increases. In [15], the adopted electrode position is basically consistent with the fetal cardiac axis.

However, all the approaches presented in the literature have two limitations. First, the signals with the highest SNR do not necessarily correspond to the optimal choice to extract the fHR. In fact, the optimal operating conditions for Independent Component Analysis (ICA), a special case of BSS, are reached by minimizing the statistical independence between components related to different sources [16].

The second limitation relates to the fetal position. Previous studies defined a-priori the optimal electrode configuration on the basis of prior knowledge on the fetal presentation (i.e., cephalic vs. breech) [8]. Such an approach is limited by the need for prior knowledge of the fetal position, and is only suitable for monitoring the final stages of pregnancy, when fetal movements are limited. Dynamic changes of the fetal position as well as inter-pregnancy differences might play a major role in determining the optimal configuration [17].

To overcome such limitations, the aim of this work is to propose a method to automatically determine the optimal electrode configuration for the fHR estimation, without prior knowledge of the fetal position. To achieve this objective, the signal analysis chain for fHR estimation, based on BSS, is taken into account.

Therefore, we consider a strategy based on Independent Component Analysis (ICA), as recently proposed by our group [18]. This strategy improves upon the algorithm proposed by Varanini et al. [19], reflecting without loss of generality the analysis chain which is mostly adopted for fHR estimation.

Our contributions are schematically presented in Fig. 1. By investigating the signal characteristics obtained with different configurations on both *in-vivo* and *in-silico* data, we first provide guidelines about the optimal electrode configuration for fHR estimation. The rationale behind our guidelines resides in the relationship between the number of independent signal sources captured by a certain electrode configuration compared to the number of available independent components, which are available for effective signal decomposition and fECG extraction. Indeed, the minimization of the number of independent components describing each source, so as not to spread each source signal over multiple components, helps reduce the number of electrodes and improve the SNR of the signals, including the fECG. Reducing the number of electrodes is crucial in long-term monitoring applications because it limits the computational complexity of the processing algorithms, prolonging battery life.

The method proposed to automatically select the optimal configuration uses a Support Vector Regression (SVR) model to predict the reliability of the resulting fHR estimation prior to its estimation, based on the acquired raw signals only. The method employs global statistical features of the raw multichannel measurements to predict the quality of the fHR estimation, assessed by a combination of F-score and root mean square error (RMSE). Such evaluation is more suitable for long-term monitoring since it avoids additional computational costs for multiple assessments of the fHR resulting from different electrode configurations.

In recent years, to make the long-term monitoring more comfortable, dry or capacitive textile electrodes embedded in garments have been proposed. For instance, Manna et al. [20] employ electrodes made of fabric to acquire the fECG signals for a home monitoring system; Signorini et al. [21] proposed a wearable system based on textile electrodes intertwined in garments to monitor fetal well-being in the last phase of pregnancy. Textile non-obtrusive and comfortable electrodes allow increasing the number of electrodes over the traditional wet electrodes. In this scenario, the proposed method can also be used to dynamically select an optimal subset of electrodes and their optimal configuration, coping with changes in the fetal position during the acquisition. Training and evaluation

of the proposed method were performed on *in-silico* data able to replicate a wide variety of possible conditions while providing a reliable ground-truth reference. Since the proposed method is the first in the literature to automatically select the optimal electrode configuration, comparison with other approaches is not yet feasible.

The paper is organized as follows: the background theory of the BSS techniques, which is fundamental to the rationale behind our approach, is reported in Section II-A. Sections II-B1 and II-C discuss the data and metrics used to design and evaluate the proposed guidelines and the automatic detection method. Sections II-D, II-E, and II-F are the core of this paper, and their main contributions are summarized in Fig. 1: Section II-D investigates whether the proposed configuration, namely the reference configuration, outperforms those employed in the literature, referred to as normal. In Section II-E, we describe the optimization of the reference configuration in terms of the number of leads, the shape of the configuration, the distance between the electrodes, and the influence of the fetal position. This optimization allows defining some guidelines for optimal electrode placement. In Section II-F, our proposed method for automatic detection of the optimal configuration is explained. Finally, Sections III and IV present the results and their discussion, respectively.

## II. MATERIALS AND METHODS

### A. Blind Source Separation Techniques for fHR Estimation.

This approach considers a set of  $n$  individual components  $\mathbf{S} = [\mathbf{s}_1, \mathbf{s}_2, \dots, \mathbf{s}_n]^T \in \mathbb{R}^{n \times Q}$ ; with  $\mathbf{s}_k = [s(T_s), \dots, s(Q \cdot T_s)]^T \in \mathbb{R}^{1 \times Q}$ ;  $k = 1, \dots, n$ ;  $n$  being the number of components needed to describe all the present sources (i.e., mECG, fECG, artifacts, noise, etc.) and  $Q$  the length of the segment;  $T_s = \frac{1}{f_s}$ , with  $f_s$  being the sampling frequency.  $\mathbf{S}$  is mixed using a matrix  $\mathbf{A} = [\mathbf{a}_{jk}] \in \mathbb{R}^{n \times m}$  as:

$$\mathbf{X} = \mathbf{A} \cdot \mathbf{S}. \quad (1)$$

Producing a set of observed mixed signals  $\mathbf{X} = [\mathbf{x}_1, \mathbf{x}_2, \dots, \mathbf{x}_m]^T \in \mathbb{R}^{m \times Q}$ , with  $\mathbf{x}_j = [x(T_s), \dots, x(Q \cdot T_s)]^T \in \mathbb{R}^{1 \times Q}$ ;  $j = 1, \dots, m$ ;  $m$  being the number of leads.

The objective of the BSS approach is to recover an approximation of the original signals  $\mathbf{S}$ , indicated as  $\hat{\mathbf{S}}$ , by the determination of an unmixing matrix  $\mathbf{B} = [\mathbf{b}_{kj}] \in \mathbb{R}^{n \times m}$  such that:

$$\hat{\mathbf{S}} = \mathbf{B} \cdot \mathbf{X}. \quad (2)$$

Several approaches have been proposed in the literature to separate the components enhancing the fECG signal, each based on different assumptions on the characteristics of the sources. Among the standard BSS methods, Principal Component Analysis seeks source components that are minimally correlated. However, the components related to the heart activity (e.g., maternal or fetal) are strongly correlated to each other, making PCA unsuitable for this work. A few exploratory studies on other BSS methods, such as singular value decomposition and non-negative matrix factorization were also reported in literature, but a large consensus is reached on the use of ICA [22]. Indeed, ICA exploits the assumptions that the source components are

non-Gaussian and statistically independent, enabling us to obtain accurate fHR estimations with low sensitivity to noise and artifacts [23]. For this reason, ICA was our choice in [18].

In this work, the unmixing matrix  $\mathbf{B}$  is obtained by applying the fastICA approach with deflationary orthogonalization [24]. This method calculates the vectors  $\mathbf{b}_k = [b_{k1}, b_{k2}, \dots, b_{km}]^T \in \mathbb{R}^{1 \times m}$  adaptively and sequentially by minimizing the mutual information between the independent components  $\mathbf{s}_k$ . As the preferred contrast function, which is defined as the (statistical) function capable of separating independent sources from a linear mixture [25], we selected the hyperbolic cosine, as it produces the most robust estimations [19].

The bioelectrical activity of the maternal heart can be represented by a three-dimensional current dipole [26], which is fixed in position but variable in magnitude and orientation [27]. Therefore, the mECG is generally formed by the combination of three independent components. Instead, the number of independent components representing the fECG is not necessarily equal to three as it depends on the fetal position; as a result, the amplitude of the fECG signal may also change. In fact, the position of the fetal heart is subject to changes during pregnancy due to fetal movements [28] and the greater the distance of the fetal heart from the electrode the lower the fECG amplitude.

The main limitation of the ICA approach is related to underdetermination, which occurs when  $n > m$  [29], making the extraction of the fECG signal often unfeasible. Indeed, BSS methods can identify a number of independent components that is at most equal to the number of mixed signals ( $m$ ), which is often insufficient to identify all the signal components. This condition is often insufficient to identify all the signal sources. In a long-term monitoring scenario, such constraint is critical as a limited number of leads is required to minimize obtrusiveness, while a high number of noise and artifact sources can affect the signal.

To tackle such limitations, we designed the electrode configuration that enhances the performance of the BSS technique by reducing the number of independent components needed to describe a specific source. In fact, a previous study suggested that the spatial location of the electrodes in the maternal abdomen influences the performance of the fHR estimation [30]. In particular, we propose to select the electrode configuration that guarantees the best trade-off between the reduction of the variability between the components related to the same source (intra-source), and the enhancement of the variability between the components related to different sources (inter-sources variability), needed to provide effective sources separation [31]. This results in an improvement in the ability of ICA to isolate the source of interest as the difference between the number of sources and the number of mixed signals is reduced [32].

As suggested by Fig. 2, this optimal trade-off is obtained by considering bipolar measurement leads with an electrode in common (reference electrode) and with the seconds close to each other (active electrodes). Such configuration is referred to as the *reference* configuration and it was employed in previous works based on BSS [33], [34] without reporting theoretical details on such a choice. For example, in [33] three bipolar leads were obtained by positioning the active electrodes in the

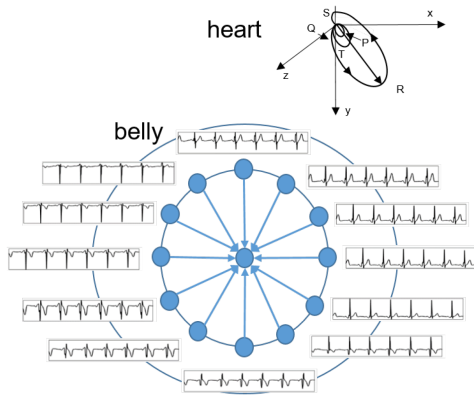


Fig. 2. mECG signals recorded by bipolar measurements in the reference configuration. The electrodes are placed on the maternal abdomen and the leads are defined by the arrows.

upper part of the belly and the reference one in the lower part. In [34], periodic component analysis ( $\pi$ CA) was applied to signals obtained by five abdominal electrodes with common reference, active ground, and one chest electrode.

Alternative to the *reference* configuration, the *normal* configuration is usually employed in studies oriented to SNR optimization and aims at maximizing the variance between the bipolar measurements [35]. There is no univocal definition of the *normal* configuration, and several versions have been presented in the literature. In this work, we consider those illustrated in Fig. 3.

## B. Dataset

**1) In-Silico Dataset:** Simulated data has been obtained with an online simulator [36]. For each 5-minute simulated recording, the position of the fetal hearts randomly changes, enabling the simulation of different fetal positions and the introduction of high variability between different subjects. Accordingly, different healthy fECG and mECG were generated and the fECG amplitude was randomly selected for each acquisition in order to simulate different gestational ages. As suggested by the literature [46], the maximum amplitude of the fECG signal is  $20 \mu\text{V}$ . mECG and fECG signals were corrupted by different sources of noise, such as acquisition noise, baseline wander, muscular noise. Five different levels of additive noise were included (0, 3, 6, 9, and 12 dB) [36]. Taking into account a wide range of SNR values and different types of noise allows evaluating the proposed work in a wide range of scenarios that can replicate the real environment. 200 different pregnant women were simulated to be part of the training dataset, and 50 for the testing set. The latter was employed only for testing the regression model. The simulated subjects are the same for the analysis conducted in Sections II-D, II-E, and II-F.

**2) In-Vivo Dataset:** Two real datasets have been included. The Seban dataset contains five abdominal measurements of 20 min each on pregnant women at full gestation (39 weeks and 4 days  $\pm$  12 days). More detailed information about the dataset acquisition can be found in [8]. The IHDB-fIHDB dataset has a total length of 9.5 h and comprises 20 abdominal measurements from eight women during labor at full term (40 weeks and 3 days

$\pm$  13 days). The dataset is fully described in [37]. The electrode positions are reported in Figs. 3(c) and 3(d), respectively. For both datasets, the reference fHR is defined by the fECG acquired through a scalp electrode.

## C. fHR Quality Metrics

The accuracy of the fHR estimation was quantified using the reference (simulated fECG in the *in-silico* dataset and scalp fECG in the *in-vivo* dataset). Each beat was classified as True Positive (TP) or False Negative (FN) if the actual R peak was detected or missed, respectively. Instead, False Positive (FP) were points that were falsely identified as R peak. An R peak was considered correctly identified if the estimated position differed less than 50 ms from the reference annotation, according to the guidelines reported in [38]. The F-score index was employed to evaluate the overall performance of the algorithm in correctly detecting R peaks:

$$\text{F-score} = \frac{2 \cdot \text{TP}}{2 \cdot \text{TP} + \text{FN} + \text{FP}} \quad (3)$$

The F-score ranges from 0 to 1, where 1 is when the detection is always correct. The accuracy and the reliability of the fHR estimation can also be evaluated with the Root Mean Square Error (RMSE), which measures the difference between the true fetal HR (fHR) and the estimation provided by the algorithm ( $\hat{\text{fHR}}$ ):

$$\text{RMSE} = \sqrt{\frac{\sum_{l=1}^{N_R} (\hat{\text{fHR}}_l - \text{fHR}_l)^2}{N_R}} \quad (4)$$

where  $l$  is the index of the  $l$ -th heartbeat and  $N_R$  is the number of heartbeats in the recording. RMSE measurement unit is ms. The smaller the RMSE, the more accurate is the fHR estimation. Low values of this metric lead to a reliable assessment of the heart rate variability (HRV), which is an important index for fetal well-being evaluation.

F-score and RMSE metrics were employed to perform quantitative comparison of the results obtained by following the analysis described in Sections II-D, II-E, and II-F. Furthermore, after verifying the normality of the result distribution with the Kolmogorov-Smirnov test [39], the Wilcoxon rank or paired t-test were used to test statistically significant differences ( $p$ -values  $<$  0.05).

## D. Identification of the Optimal Configuration Type

To determine the most suitable configuration to estimate the fHR with BSS techniques, a comparison between reference and normal configurations was performed on both the *in-vivo* (Seban, IHDB-fIHDB) and *in-silico* datasets. For each set of signals obtained with the different configurations, the algorithm described in [18] was applied to estimate the fHR. The position of the electrodes for the reference and normal configurations are reported in Fig. 3 for both the *in-vivo* and *in-silico* datasets. The arrows indicate the bipolar leads. For what concerns the *in-silico* dataset, two configurations have been evaluated: the first is formed by eight leads and the second by four. *In-vivo*

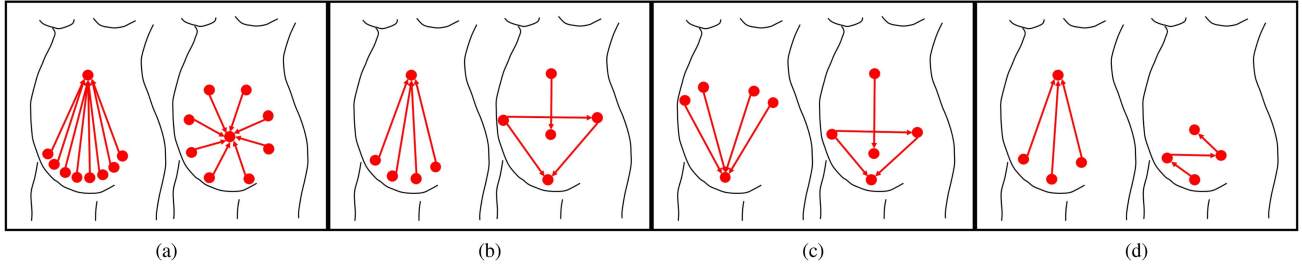


Fig. 3. Electrode configurations for *in-silico* and *in-vivo* data. For each dataset, the reference (left) and the normal (right) configuration are depicted. a) *In-silico* dataset - eight leads configuration. b) *In-silico* dataset - four leads configuration. c) *In-vivo* Seban dataset. d) *In-vivo* IHDB-fIHDB dataset.

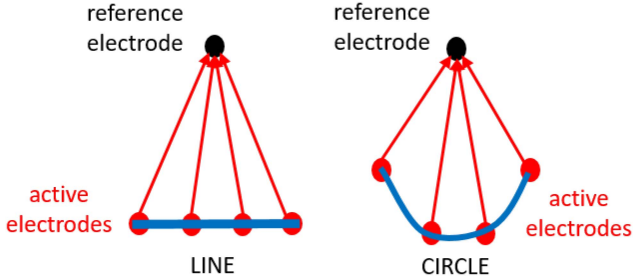


Fig. 4. Active electrode placed on a line or on a semi-circle.

Seban datasets have five electrodes, i.e., four bipolar leads, while the recordings from the IHDB-fIHDB datasets are composed by four electrodes only. The fetal position is cephalic for all the *in-vivo* acquisitions, while it is unknown for the *in-silico* dataset.

### E. Optimization of the Reference Electrode Configuration to Define Guidelines

After establishing the superiority of the reference configuration over the normal configuration (as detailed in Section III), we optimized *in silico* its characteristics in terms of number of leads, position of electrodes, distance between electrodes. For this analysis, the position of the fetus is random and unknown. Finally, the orientation over the maternal abdomen is also evaluated according to the position of the fetus. The electrode configuration that provided the most accurate estimation of the fHR with the selected BSS technique [18] was then determined.

**1) Minimum Number of Leads:** in this study, we simulated a scenario where the acquired signals are composed of fECG, mECG, and superposed noise only. We determined the minimum number of electrodes as the value after which there are no more significant improvements in the estimation accuracy by increasing the number of leads.

**2) Position of the Active Electrodes:** we considered two different scenarios: with the active electrodes on the same line, and with the active electrodes over a semi-circle, as shown in Fig. 4. In this work, we called active electrodes those opposite to the reference electrode, marked in black in Fig. 4.

**3) Distance Between Electrodes:** as previously discussed, the distance between the electrodes plays a fundamental role in the ability of ICA to separate the components. If the electrodes

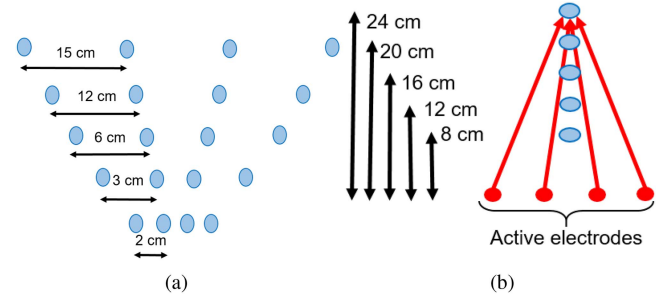


Fig. 5. a) Active electrodes position. The proximity levels are: 15 cm; 12 cm; 6 cm; 3 cm; 2 cm. b) Reference electrodes position. The distance levels are: 24 cm; 20 cm; 16 cm; 12 cm; 8 cm.

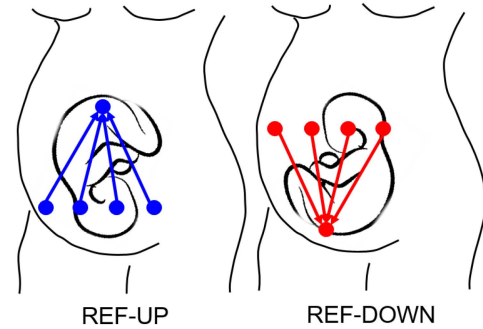


Fig. 6. Electrode configuration REF-UP and REF-DOWN.

are too close, the variability between the leads is too low, which makes the separation of the sources challenging. We evaluated both the distance between the active electrodes (proximity measurement) and between the active electrodes and the reference one (distance measurements). We considered the five proximity levels shown in Fig. 5(a). To evaluate the optimal proximity level, we chose a fixed distance of 16 cm between the reference and the active electrode.

The five evaluated distance levels are reported in Fig. 5(b). To perform such evaluation, we chose a fixed distance of 8 cm between the actives electrodes.

**4) Influence of the Fetal Position:** we compared, through F-score and RMSE metrics, a reference configuration with reference electrode on the upper part of the belly (the REF-UP) and with the reference electrode on the lower part of the belly (REF-DOWN) for breech and cephalic positions considered separately. The considered configurations are shown in Fig. 6.

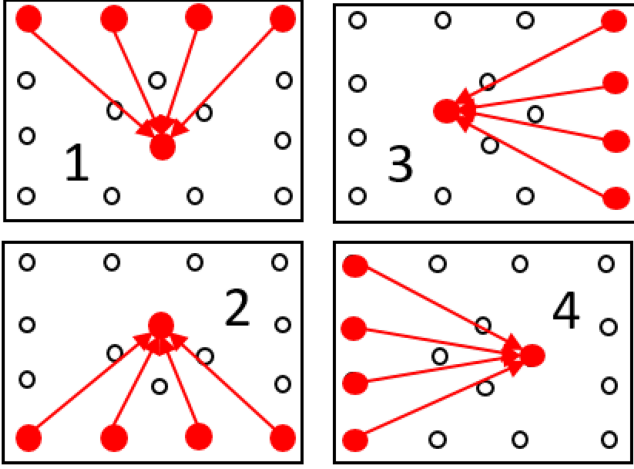


Fig. 7. The electrode configurations considered. The distance between horizontal and vertical positions is equal to 8 cm.

### F. Automatic Selection of the Optimal Electrode Configuration With Unknown Fetal Position

Following the analysis described in Section II-E, we established the guidelines, to optimally position the electrodes over the maternal belly. Such optimal configuration was used in the following analysis.

A final aspect to be taken into account in order to obtain the best fHR estimation is the automatic selection of the best electrode configuration, which depends on both the quality of the acquired signals and the fetal position. Our proposed system can automatically assess the quality of a configuration without requiring any knowledge about the fetal position. In this way, it is possible to dynamically determine the best electrode positions, even if the position of the fetus is unknown and the quality of the signals changes due to motion artifacts or loss of contact between the electrode and the skin.

To that end, we considered the *in-silico* dataset and we simulated the signals coming from a grid of 16 electrodes positioned on the maternal abdomen. The inter-electrode distance in such a grid is defined following the recommendations derived from the results obtained with the tests in Sections II-D and II-E. Four optimal reference configurations were selected, as shown in Fig. 7, with each one being the optimal configuration for one of the most common fetal presentations (1 - breech, 2- cephalic, 3 - side right, 4 - side left).

We quantified the quality of each configuration in terms of fHR estimation by means of a *hybrid* index (HI) obtained by combining RMSE and F-score metrics according to:

$$HI = \frac{RMSE}{F\text{-score}} \quad (5)$$

This index is strongly related to the RMSE value; however, by taking into account F-score values, we can improve the discrimination between the configurations providing accurate and non-accurate estimation of the fHR. Lower HI indicates fHR estimations that are closer to the real fHR; in particular, we considered  $HI < 25$  to indicate a good fHR estimation. Such

threshold was established to obtain an RMSE for the fHR estimation lower than 25 ms.

**1) Feature Extraction From Raw Data:** for each configuration, we considered eleven global statistical features obtained on four 10-s raw bipolar measurements. The features can be subdivided into two groups. In the first group, the features are extracted for each single lead independently: Kurtosis (K), Skewness (SK), Mean (M), Variance (V), Approximate Entropy (ApEn), Sample Entropy (SampEn). Therefore, the corresponding feature related to the configuration is computed by averaging the values obtained for each lead. In the second group, the features are obtained considering two different leads: Pearson Correlation coefficient (PCC), CrossEntropy (CrossEn), Mutual Information (MI), Coherence (CH), CrossCorrelation (CC). In this case, the configuration feature is computed by averaging the features related to all the possible pairs obtained by combining the four leads. In total, 11 features are extracted. For more details on the features, we remand to the references [39], [40].

**2) Support Vector Regression (SVR):** to predict the HI by means of the features extracted from the raw data, a Support Vector Regression (SVR) model was employed. This way, we implicitly assumed the value of HI, which is the dependent variable, to be described by a non-linear combination of the statistical features, i.e., the independent variables ( $\mathbf{x}$ ). SVR is a non-parametric technique which finds the model that fits the data guaranteeing an approximation error lower than. SVR maps the input vector into a feature space of higher dimension and identifies the hyperplane  $f(\mathbf{x}) = \mathbf{w}^T \cdot \mathbf{x} - b = 0$  that deviates the observations (HI) by a value not larger than for each training point  $\mathbf{x}$ , and that at the same time is as flat as possible. It is possible that no function  $f(\mathbf{x})$  exists to satisfy the error constraint for all the observations. To deal with otherwise infeasible constraints, slack variables  $\xi$  and  $\xi^*$  are introduced for each point [41]. This approach is similar to the soft margin concept in Support Vector Machine (SVM) classification as the slack variables allow regression errors to exist up to the value of  $\xi_n$  and while still satisfying the required conditions. The related objective function is given as

$$\min \frac{1}{2} \|\mathbf{w}\|^2 + C \sum_{i=1}^N (\xi_i - \xi_i^*) \quad (6)$$

subject to:

$$\begin{aligned} HI_i - \mathbf{w}^T \mathbf{x}_i + b &\leq \epsilon + \xi_i^*, \quad i = 1, \dots, N \\ (\mathbf{w}^T \mathbf{x}_i + b) - HI_i &\leq \epsilon + \xi_i, \quad i = 1, \dots, N \\ \xi_i, \xi_i^* &\geq 0 \end{aligned} \quad (7)$$

The constant  $C$  is a regularization hyper-parameter that controls the penalty imposed on observations that lie outside the margin and helps to prevent over-fitting.  $N$  is the number of subjects considered in the training phase.

If the data are not linearly separable, like in the problem under consideration, a kernel trick can be applied for mapping the data to a higher-dimensional space, achieving more effective data separation [42]. In this work, we used a Radial Basis Function

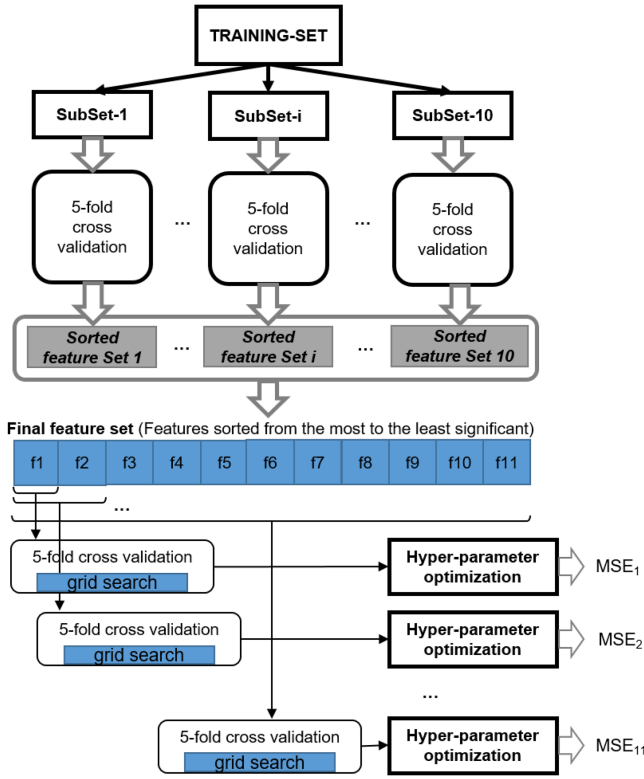


Fig. 8. Schematic representation of the selection procedure to determine the sorted feature set and of the optimization of the hyper-parameters.

(RBF) kernel defined as:

$$K(\mathbf{x}, \mathbf{x}') = (\Phi(\mathbf{x}) \cdot \Phi(\mathbf{x}')) = \exp(-\gamma \|\mathbf{x} - \mathbf{x}'\|^2), \quad (8)$$

$\gamma$  is RBF kernel parameter and  $\Phi$  is the map.

**3) SVR Optimization:** In this section, the optimization of the SVR is described in terms of the selection of the most significant features and the optimal values of the model hyper-parameters (i.e.,  $C$ ,  $\gamma$ , and  $\epsilon$ ) according to the schematic representation presented in Fig. 8. The optimization was performed on the training set, which includes 80% of the subjects from the entire *in-silico* dataset, randomly selected.

**a) Feature Sorting:** We divided the training-set in ten different subsets, each one including 50% of the training-set data through random selection. On each subset, 5-fold cross-validation forward feature sorting was performed to obtain the sorted feature set: starting from an empty feature set, at each iteration the feature contributing to the best improvement in performance was added to the selected feature set. The performance was assessed in terms of Mean Square Error (MSE):

$$\text{MSE} = \frac{\sum_{i=1}^N (\hat{\text{HI}}_i - \text{HI}_i)^2}{N} \quad (9)$$

where  $(\hat{\text{HI}})$  is the prediction of the real value (HI) provided by the SVR model.

The iterations were repeated until no more features were available. Such procedure was repeated for each of the 10 training subsets to improve the result generalizability. Indeed,

we obtained the final sorting of the 11 features from the most to the least significant  $[f_1, f_2, \dots, f_{11}]$  by sorting the averaged feature ranking for the 10 subsets.

**b) Hyper-parameter optimization:** The values of the hyper-parameters ( $C$ ,  $\gamma$  and  $\epsilon$ ) were optimized for each feature set formed by an increasing number of features based on the final averaged sorting (i.e.,  $[f_1]$ ,  $[f_1, f_2]$ ,  $\dots$ ,  $[f_1, f_2, \dots, f_{11}]$ ) as shown in Fig. 8. The hyper-parameter optimization was performed by means of a full grid search embedded in a 5-fold cross-validation over the full training set (80% of the subjects). The adopted ranges for the grid search were the exponentially growing sequences  $[10^{-3}, 10^{-2}, \dots, 10^3]$  for the constant  $C$ ,  $[2^{-3}, 2^{-2}, \dots, 2^3]$  for the kernel parameter  $\gamma$  and  $[10^{-4}, 10^{-3}, \dots, 10^2]$  for  $\epsilon$ . In this way, we obtained 11 different regression models, each referring to a different set of features (i.e.,  $[f_1]$ ,  $[f_1, f_2]$ ,  $\dots$ ,  $[f_1, f_2, \dots, f_{11}]$  with the related optimized hyper-parameters. The performance of such regression models was again defined according to the MSE (9).

**c) Feature selection:** The dimension of the optimal feature set and the related optimized hyper-parameters were selected according to the overall minimization of the MSE. Feature selection enables selecting a subset of relevant features by disregarding features that are either redundant or irrelevant, without incurring in significant loss of information. The selection has several advantages, such as reducing of the model complexity, which facilitates its interpretation; increasing the prediction accuracy, if the selected subset is robust; mitigating over-fitting problems; reducing the model training time [4].

**4) Assessment of Prediction Quality:** The proposed approach was evaluated on the test set, which consist of 50 simulated pregnant women (20% of the entire *in-silico* dataset) that were not employed for the optimization of the configuration characteristics and the training of the SVR model. The aim of the regression model is to predict, for each configuration, the HI value. Configurations showing  $\text{HI} < 25$  are considered good while the others are considered bad configurations. According to this threshold, each configuration can be classified as True Good (TG) or False Bad (FB), if a good configuration is recognized or missed, respectively. False Good (FG) and True Bad (TB) are the bad configurations that are wrongly or correctly identified, respectively. Therefore, the performance of the regression model can be assessed in terms of classification performance according to the following metrics:

- Accuracy (AC):

$$\text{AC} = \frac{\text{TG}}{\text{TG} + \text{FG} + \text{TB} + \text{FB}} \cdot 100 \quad (10)$$

- Sensitivity (SE):

$$\text{SE} = \frac{\text{TG}}{\text{TG} + \text{FB}} \cdot 100 \quad (11)$$

- Specificity (SP):

$$\text{SP} = \frac{\text{TB}}{\text{FG} + \text{TB}} \cdot 100 \quad (12)$$

Finally, to evaluate the performance of the regression model in identifying the configuration leading to the best HI index, the

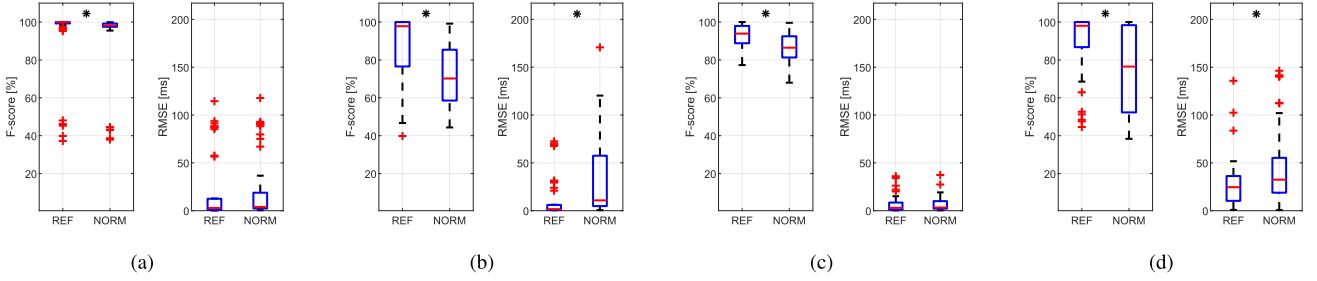


Fig. 9. Boxplots showing the performance analysis for both F-score (left) and RMSE (right) metrics. a) *In-silico* dataset - eight leads configuration. b) *In-silico* dataset - four leads configuration. c) *In-vivo* Seban dataset. d) *In-vivo* IHDB-fIHDB Datasets. \* Statistically significant difference ( $p < 0.05$ ) between the REF and NORM configurations with the Wilcoxon signed rank test.

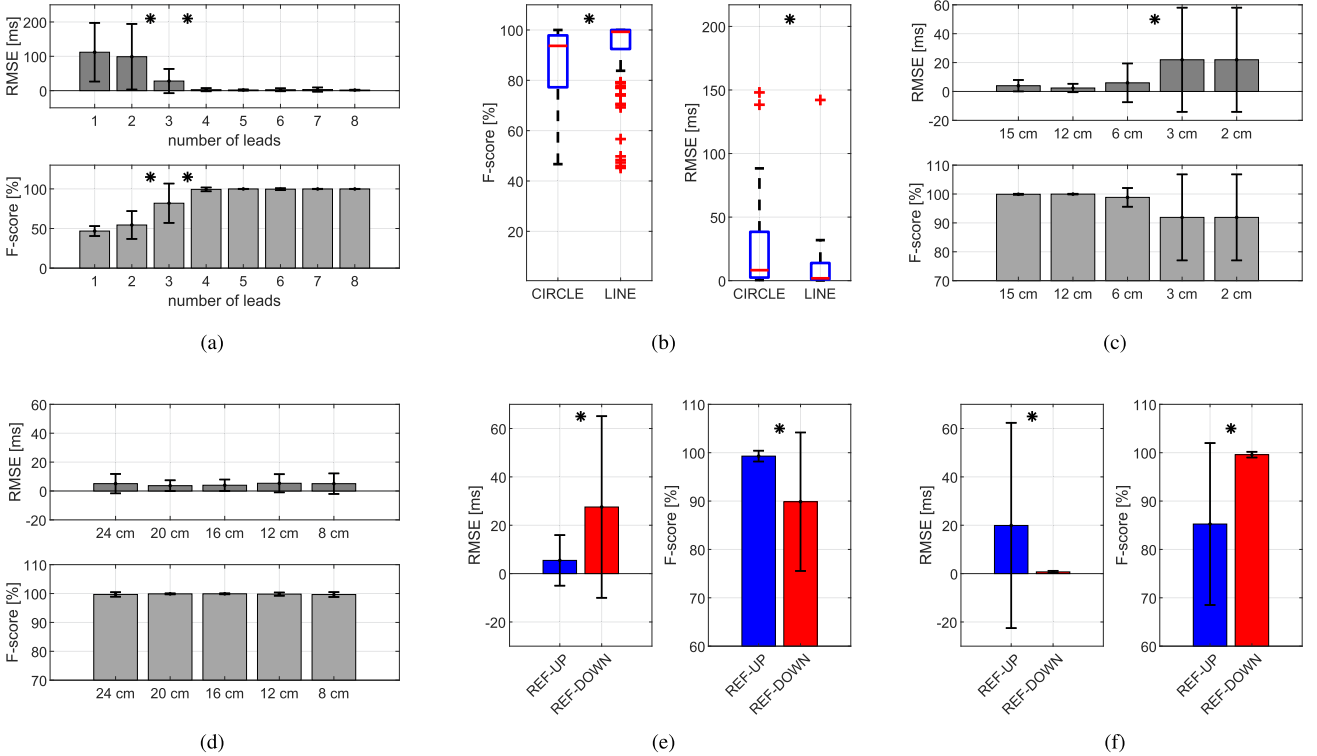


Fig. 10. a) Performance analysis according to the number of leads for F-score (down) and RMSE (top) metrics. b) Boxplots showing the performance analysis for both F-score (left) and RMSE (right) metrics according to the position of the active electrodes (circle or line). c-d) Performance analysis for F-score (down) and RMSE (top) metrics, according to c) the distance between the active electrodes and d) the distance between reference and active electrodes. e-f) Performance analysis (mean and standard deviation) according to REF-UP and REF-DOWN configuration placement and the fetus position, i.e., cephalic (e) and breech (f), for F-score (right) and RMSE (left) metrics. \* Statistically significant difference ( $p < 0.05$ ) between the REF and NORM configurations with the Wilcoxon signed rank test.

Percentage of Correct identification (PC) was computed as:

$$PC = \frac{CI}{N} \cdot 100 \quad (13)$$

where, CI quantifies the amount of correct identifications and  $N$  is the total number of evaluated subjects.

### III. RESULTS

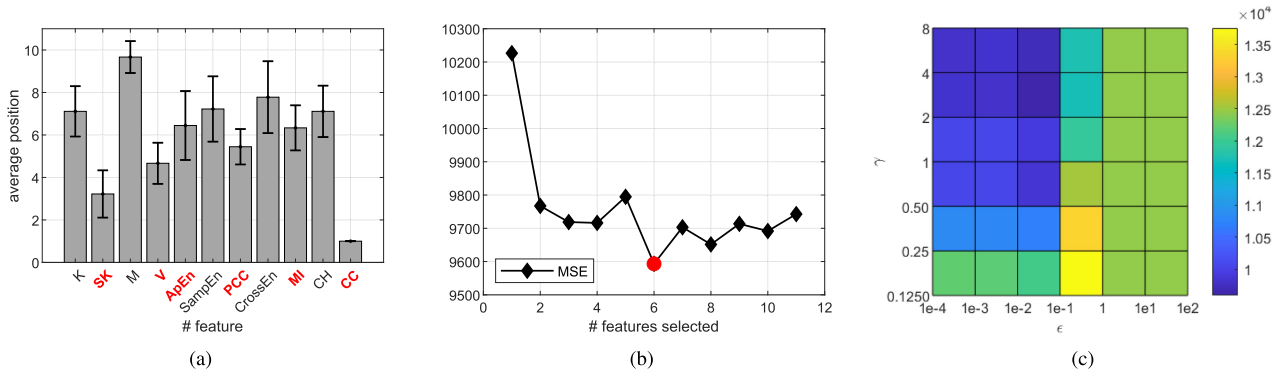
Fig. 9 shows the comparison of the fHR estimation performance, both in terms of F-score and RMSE, between the reference and normal configurations. The comparison is performed both on *in-silico* data, Figs. 9(a) and 9(b), and *in-vivo* data, Figs. 9(c) (Seban) and 9(d) (IHDB-fIHDB).

Fig. 10(a) shows the performance changes for increasing number of leads. Significant improvements are obtained in terms of increase of the F-score and decrease of the RMSE until the number of leads is equal to four. After this value, increasing the number of leads does not introduce any significant improvement.

Fig. 10(b) reports the comparison between positioning the active electrodes on a semi-circle or on a line. The evaluation was performed *in silico*. Electrodes placed on a line enable to obtain significantly better performance in terms of both RMSE and F-score.

Figs. 10(c) and 10(d) investigate the influence on the fHR estimation of the distance between the active electrodes (proximity measurement) and between the reference and active electrodes





**Fig. 11.** a) Average ranking of the features in the feature set. The feature set is sorted increasingly according to the average rank as follows: Cross-Correlation (CC), Skewness (SK), Variance (VA), Pearson Correlation Coefficient (PCC), Mutual Information (MI), Approximate Entropy (ApEn), Kurtosis (K), Coherence (CO), Sample Entropy (SampEn), Cross-Entropy (CrossEn), Mean (M). The features in red are those selected as the best feature set. b) MSE obtained for the generalized feature set and the optimal hyper-parameters selection. The red circle indicates the minimum value obtained with the best features set of six elements. c) Mean Square Error (MSE) as function of  $\gamma$  and  $\epsilon$ , with  $C = 0.1$ , for the optimal feature set.

**TABLE I**

EVALUATION METRICS, BOTH IN TERMS OF PREDICTION ACCURACY (MSE) AND CLASSIFICATION PERFORMANCE, I.E., ACCURACY (AC), SENSITIVITY (SE), SPECIFICITY (SP), FOR INCREASING ELEMENTS OF THE SORTED FEATURE SET. THE PERFORMANCE IS COMPUTED CONSIDERING THE OPTIMAL VALUES OF THE HYPER-PARAMETERS AND IS ASSESSED ON THE TRAINING SET

Num. Features	Feature Set	MSE	AC [%]	SP [%]	SE [%]
1	CC	1.02e4	77.1	80.7	70.9
2	CC - SK	0.9e4	80.5	89.6	64.8
3	CC - SK - V	0.97e4	81.2	94.0	59.4
4	CC - SK - V - PCC	0.97e4	81.1	94.4	58.4
5	CC - SK - V - PCC - MI	0.98e4	81.0	93.8	59.1
<b>6</b>	<b>CC - SK - V - PCC - MI - ApEn</b>	<b>0.95e4</b>	<b>82.1</b>	<b>89.3</b>	<b>66.5</b>
7	CC - SK - V - PCC - MI - ApEn - K	0.97e4	80.6	90.1	64.5
8	CC - SK - V - PCC - MI - ApEn - K - CO	0.96e4	81.7	86.5	73.6
9	CC - SK - V - PCC - MI - ApEn - K - CO - SampEn	0.97e4	80.9	87.7	69.3
10	CC - SK - V - PCC - MI - ApEn - K - CO - SampEn - CrossEn	0.97e4	80.7	87.9	68.6
11	CC - SK - V - PCC - MI - ApEn - K - CO - SampEn - CrossEn - M	0.97e4	79.9	88.1	65.9

(distance measurement), respectively. A significant improvement in fHR performance is obtained only by increasing the distance between active electrodes from 3 to 6 cm. Instead, no significant improvement in terms of both F-score and RMSE metrics is achieved by varying the distance between the actives and reference electrodes.

The results obtained in Figs. 10(a), 10(b), 10(c), and 10(d) have been obtained without knowing the position of the fetus. On the contrary, the position of fetus is known in Figs. 10(e) and 10(f) and the results highlight that placing the reference electrode on the upper or lower part of the mother's abdomen influences the estimation performance in terms of both F-score and RMSE. In fact, placing the active electrodes close to the head of the fetus, i.e., REF-UP for cephalic presentation (Fig. 10(e)) and REF-DOWN for breech presentation (Fig. 10(f)) enables significantly better performance.

Since the fetal position is unknown for most of the pregnancy, in Section II-F an SVR for automatic prediction of the optimal configuration according to the optimization of a quality index is proposed. The optimization of the SVR prediction model involves the determination of the optimal number of features and the values of the SVR hyper-parameters that enable the

minimization of the difference between  $\hat{H}I$  and  $H_I$ . Fig. 11 reports the results, based on the training dataset, used to achieve this purpose. In particular, Fig. 11(a) shows the average ranking (with standard deviation) of all the features, which is employed to sort the features from the most to the least significant.

Fig. 11(b) reports the MSE obtained by increasing the number of features and considering the related optimal hyper-parameter values. According to the minimization of the MSE metric, the optimal feature set is formed by six features, which are: cross-correlation, skewness, variance, Pearson correlation coefficient, mutual information, and approximate entropy. Additionally, Fig. 11(c) shows the best hyper-parameter values ( $C = 0.1$ ,  $\gamma = 2$ , and  $\epsilon = 0.01$ ) for the optimal feature set.

Table I reports the evaluation metrics, described in Section II-F4, obtained in the training set by increasing the number of features considered. In this table, the optimal feature set is highlighted in bold, which, in addition to minimizing the prediction error, enables to reach an accuracy equal to 82.1%.

Finally, the SVR model and its ability to predict the outcome of the processing algorithm was evaluated on the test set. The values of the evaluation metrics, described in Section II-F4, are reported in Table II.

TABLE II

ACCURACY (AC), SENSITIVITY (SE), SPECIFICITY (SP) AND THE PERCENTAGE OF CORRECT IDENTIFICATION (PC) EVALUATED ON THE TEST SET BY USING THE SVR OPTIMIZED DURING THE TRAINING PHASE. ALSO, THE FEATURE SET AND THE VALUES OF THE HYPER-PARAMETERS ARE REPORTED

Num. Features	Feature Set	Hyper-parameter			AC [%]	SP [%]	SE [%]	PC [%]
		$C$	$\epsilon$	$\gamma$				
6	CC - SK - V - PCC - MI - ApEn	0.1	0.01	2	80.9	87.9	70.0	92.2

#### IV. DISCUSSION

In this work, a pipeline was proposed to automatically optimize the electrode configuration in terms of the number and position of the electrodes on the maternal abdomen. Such optimal configuration allows reaching the optimal estimation of the fHR by means of the algorithm described in [18] and, more generally, based on the blind source separation technique.

##### A. Identification of the Optimal Configuration Type

Fig. 9 shows that the reference configuration was always able to achieve a significantly better fHR estimation except for the Seban dataset, where the assessed RMSE was on average  $< 10$  ms for both normal and reference configurations. In fact, positioning the electrodes following the reference configuration makes the contribution of one of the three independent components that describe the mECG signal negligible, while at the same time enhancing the contribution of the other two. This has two advantages, particularly relevant in case the number of leads is limited. Firstly, it improves the identification of the mECG signal, facilitating its removal from the acquired signals. This is a fundamental step in all non-invasive fECG analysis, as effective removal of mECG is required to obtain an accurate detection of fHR. Secondly, by reducing the number of components needed to describe the mECG, there are more components available to map the fECG and other noise sources. This results in the identification of low-amplitude fECG, even in the presence of noise or artifacts.

Figs. 9(c) and 9(d) show the results obtained in the *in vivo* dataset. The data were acquired at the end of pregnancy, when the fECG signal has the maximum amplitude and the SNR has the highest value. In some cases, the fECG can even be visually recognized, presenting amplitude greater than noise. If at least four bipolar leads are available, i.e., at least four independent components can be identified, the fECG can be easily isolated, regardless of the number of components needed to represent the mECG; the electrode position has then limited influence on the fECG extraction. For this reason, considering the data from the Seban database (Fig. 9(c)), the fHR estimate provided by the reference configuration is not significantly different from that provided by the normal configuration. Instead, the reference configuration provides significant improvements when the available leads are less than four, as in the IHDB-fIHDB database (Fig. 9(d)).

*In silico* (Figs. 9(a) and 9(b)), the range of variation of the fECG amplitude is wide, so as to simulate different stages of pregnancy. Regarding the configuration formed by eight leads (Fig. 9(a)), the reference configuration enables us to obtain

significantly better performance in terms of F-score metric. On the other hand, the RMSE values are not significantly different, even if the dispersion of the RMSE values obtained with the normal configuration is greater than that obtained with the reference configuration. When these results are compared with those obtained with only four leads (Fig. 9(b)), the difference between the normal and the reference configurations is less marked. Indeed, the reduction in the number of components obtained by the reference configuration becomes less beneficial when the number of observations is high, like with eight leads. On the other hand, when the number of leads is limited as shown in Fig. 9(b), where the leads are only four, the results obtained by applying the selected algorithm to signals acquired by the reference configuration outperform the results obtained from signals recorded by the normal configuration both in terms of R peak position and fHR estimation. Therefore, the reference configuration can help recognize the fECG when the acquisition conditions are challenging, due to a reduced number of available signals and lower SNR.

##### B. Optimization of the Reference Configuration Characteristics

After established that the reference configuration is more suitable than the normal configuration for fHR estimation, we optimized the reference configuration characteristics in terms of number of leads, distance between the electrodes, shape, and electrode placement. For what concerns the number of leads, the evaluation was done *in silico*, where the experiments were performed without high amplitude artifacts due to movements that can be detected by the ICA as sources. In this way, we consider that our signal is composed by a limited number of main sources, i.e. maternal and fetal heart activity, muscular and respiration noise, and acquisition noise. Therefore, by leveraging the strategy presented in this paper, with an electrode configuration that minimizes the number of fECG and mECG components, along with our ICA-based denoising algorithm [18], we consider four leads as sufficient for fetal R-peaks detection (Fig. 10(a)).

The proposed method is not optimal when the number of independent sources in the signal is high, e.g. due to motion artifacts in extramural monitoring. This can be tackled by adjusting the strategy proposed in this work to more electrodes while exploiting the same ICA-based signal processing approach. Indeed, the adaptive segmentation of the signals described in [18] limits the number of sources due to motion artifacts in the same ICA segment. In this way, the number of sources for each adaptive segment is kept limited, enabling the effective isolation of the fECG even if the acquired signals are corrupted by a larger number of decorrelated motion artifacts (independent sources).

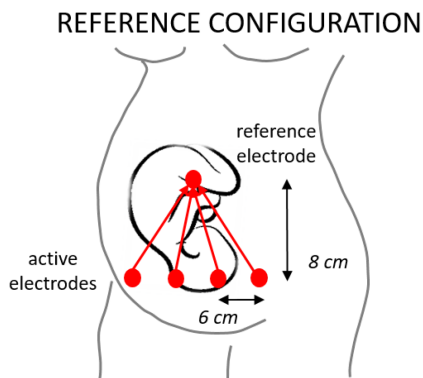


Fig. 12. Guidelines for the optimal electrode configuration, which consists of a reference configuration formed by four leads obtained by placing the active electrodes along a horizontal line at a mutual distance of 6 cm. The active electrodes are close to the head of the fetus, and the reference electrode is positioned on the opposite side of the maternal abdomen at a distance 8 cm from the active electrodes.

Placing the electrodes on a line produces significantly better performance than placing the active electrodes on a semi-circle (Fig. 10(b)). Figs. 10(c) and 10(d) present the results for the investigated distances between the electrodes. For what concerns the active electrodes, their minimum mutual distance for highly accurate performance is 6 cm. Indeed, reducing the distance makes the signals acquired by each lead too similar, hampering the separation of independent components by ICA. Instead, increasing the distance between the reference electrode and the active electrodes from 8 to 24 cm does not lead to any improvement, suggesting a distance of 8 cm to be the most suitable for the intended applications, limiting the obtrusiveness of the measurement setup.

According to the results presented in Figs. 10(e) and 10(f), the best option is positioning the active electrodes close to the head of the fetus; therefore, the best position is REF-UP, i.e., the reference electrode placed on the upper part of the belly, for cephalic presentation, and REF-DOWN, reference in the lower part of the belly, for breech presentation. Following this suggestion, the amplitude of the fECG signal is enhanced, and the number of independent components required to describe the fECG is reduced. This combination facilitates the detection of the fHR.

Summarizing, our results suggest that the optimal electrode configuration consists of a reference configuration with four leads obtained by positioning the active electrodes along a horizontal line at a mutual distance of at least 6 cm; the reference electrode is placed on the opposite side of the maternal abdomen at a distance of at least 8 cm from the active electrodes. Furthermore, we also observed that the best electrode configuration features the active electrodes close to the fetal head. The optimal configuration is defined here according to the performance obtained by the processing algorithm described in [18] for fHR assessment. The proposed guidelines, which are summarized in Fig. 12, ease both the extraction of the fECG and the estimation of the fHR as it combines the reduction of the number of independent components needed to describe the ECG signals with an enhancement of the fECG amplitude.

### C. Automatic Selection of the Optimal Electrode Configuration With Unknown Fetal Position

Table II reports the performance of the proposed automatic optimal configuration detector evaluated in the test set. The data forming this set are completely independent of those used to define our guidelines, optimize the model parameters, and train the SVR. This was to ensure a fair evaluation of our method. As shown in Table II, the accuracy of the prediction model is 80.9%, only slightly lower than that obtained on the validation set (82.1%, reported in Table I). This indicates that the model is generalizable. Accuracy describes the overall performance of the model and takes into account both types of errors: FG and FB. The latter is more frequent than the former. Indeed, the Specificity is higher than the Sensitivity, showing that the bad configurations are correctly classified more easily than the good configurations.

Considering the purpose of the current work, aiming at the selection of the electrode configuration resulting in the best fHR estimation, the FB error is less critical than the FG error. Indeed, if a bad configuration is wrongly recognized as good and employed to acquire the multichannel signals, the quality of fHR estimation will be poor with consequent deterioration of the monitoring quality. On the other hand, if a good configuration is wrongly recognized as bad, another good configuration will be selected without significant deterioration of the monitoring performance.

The goal of pre-selecting an optimal configuration among a multitude of configurations made available by an electrode grid is clearly accomplished, as confirmed by the high value of the PC metric, with more than 92% of the subjects where the best configuration was correctly identified.

### D. Limitations

The main limitation of this work is in that the proposed automatic optimal configuration detection method, based on SVR, is trained and validated on *in-silico* data only. This scenario is simpler than reality, as it disregards the variety of motion artifacts that typically corrupt long-term monitoring. Furthermore, in the simulator, the fetus is approximated with a current spherical dipole. Therefore, the simulations lack fetal movements because they cannot be reproduced with sufficient reliability. Both types of artifacts could degrade the detection performance reported in this work. However, due to the complexity of pregnancy and the difficulty in obtaining information about the fetus, such as position and reliable estimation of the fHR (especially during the vernix caseosa period), the use of *in-silico* data enables us to provide an accurate ground-truth reference and a large number of subjects, while considering a wide variety of different conditions and scenarios. In future developments, the proposed method will also be applied and validated in real pregnancies.

## V. CONCLUSION

To conclude, the proposed method provides for the first time indications about the most suited electrode configuration for fHR

monitoring by multichannel electrophysiological recording, taking into account the characteristics of the source signals in combination with the algorithms employed for fHR estimation, and dynamically adapting to the fetal presentation.

The proposed method, based on SVR, can predict in advance the accuracy of the fHR estimation based on features extracted from the raw data, prior to performing complex fHR estimations. When more electrodes are available, the automatic selection of the best 5-electrode configuration proposed in this manuscript is the optimal solution to take advantage of the 16-channel recording while keeping the computational cost low. Indeed, the optimal configuration is made up of only four leads that ensure lightweight processing.

The proposed solution, beyond being flexible, robust, and lightweight, can handle the change in fetal position and manage signal degradation, ensuring accurate and reliable estimation of the fHR also during wearable, long-term monitoring applications.

## REFERENCES

- [1] C. V. Ananth and A. M. Vintzileos, "Maternal-fetal conditions necessitating a medical intervention resulting in preterm birth," *Amer. J. Obstet. Gynecol.*, vol. 195, no. 6, pp. 1557–1563, 2006.
- [2] D. Ayres-de Campos et al., "FIGO consensus guidelines on intrapartum fetal monitoring: Cardiotocography," *Int. J. Gynecol. Obstet.*, vol. 131, no. 1, pp. 13–24, 2015.
- [3] P. Hamelmann et al., "Doppler ultrasound technology for fetal heart rate monitoring: A review," *IEEE Trans. Ultrasonics, Ferroelectrics, Freq. Control*, vol. 67, no. 2, pp. 226–238, Feb. 2020.
- [4] G. Clifford et al., "Clinically accurate fetal ECG parameters acquired from maternal abdominal sensors," *Amer. J. Obstet. Gynecol.*, vol. 205, no. 1, pp. 47–e1–47.e5, 2011.
- [5] V. S. Kurtadikar and H. M. Pande, "Comprehensive study of fetal monitoring methods for detection of fetal compromise," in *Machine Learning for Predictive Analysis*, Berlin, Germany: Springer, 2021, pp. 153–162.
- [6] D. A. Ramlı, Y. H. Shiong, and N. Hassan, "Blind source separation (BSS) of mixed maternal and fetal electrocardiogram (ECG) signal: A comparative study," *Procedia Comput. Sci.*, vol. 176, pp. 582–591, 2020.
- [7] C. Hummersone, T. Stokes, and T. Brookes, "On the ideal ratio mask as the goal of computational auditory scene analysis," in *Blind Source Separation*. Berlin, Germany: Springer, 2014, pp. 349–368.
- [8] M. J. Rooijackers et al., "Influence of electrode placement on signal quality for ambulatory pregnancy monitoring," *Comput. Math. Methods Med.*, vol. 2014, 2014, Art. no. 960980.
- [9] N. Fauzani et al., "Two electrodes system: Performance on ECG FECG and EMG detection," in *Proc. IEEE Student Conf. Res. Develop.*, 2013, pp. 506–510.
- [10] N. Marchon and G. Naik, "Electrode positioning for monitoring fetal ECG: A review," in *Proc. Int. Conf. Inf. Process.*, 2015, pp. 5–10.
- [11] J. Roche and E. Hon, "The fetal electrocardiogram: V comparison of lead systems," *Amer. J. Obstet. Gynecol.*, vol. 92, no. 8, pp. 1149–1159, 1965.
- [12] B. Murmann, "Limits on ADC power dissipation," in *Analog Circuit Design*, Berlin, Germany: Springer, 2006, pp. 351–367.
- [13] R. Vullings et al., "Dynamic segmentation and linear prediction for maternal ECG removal in antenatal abdominal recordings," *Physiol. Meas.*, vol. 30, no. 3, pp. 291–307, 2009.
- [14] S. M. Martens et al., "A robust fetal ECG detection method for abdominal recordings," *Physiol. Meas.*, vol. 28, no. 4, pp. 373–388, 2007.
- [15] J.-M. Zhang et al., "Some regularity on how to locate electrodes for higher fECG SNRS," *Chin. Phys. B*, vol. 24, no. 3, 2015, Art. no. 038702.
- [16] A. Hyvärinen and E. Oja, "Independent component analysis: Algorithms and applications," *Neural Netw.*, vol. 13, no. 4/5, pp. 411–430, 2000.
- [17] R. Martinek et al., "Non-invasive fetal monitoring: A maternal surface ECG electrode placement-based novel approach for optimization of adaptive filter control parameters using the LMS and RLS algorithms," *Sensors*, vol. 17, no. 5, 2017, Art. no. 1154.
- [18] A. Galli et al., "Dedicated algorithm for unobtrusive fetal heart rate monitoring using multiple dry electrodes," *Sensors*, vol. 21, no. 13, 2021, Art. no. 4298.
- [19] M. Varanini et al., "An efficient unsupervised fetal QRS complex detection from abdominal maternal ECG," *Physiol. Meas.*, vol. 35, no. 8, pp. 1607–1619, 2014.
- [20] S. Manna, N. Sriiram, and P. Pandian, "Prototype of home based multichannel wearable wireless fetal ecg monitoring system," in *Proc. IEEE Int. Conf. Electron., Comput. Commun. Technol.*, 2021, pp. 1–4.
- [21] M. G. Signorini et al., "Antepartum fetal monitoring through a wearable system and a mobile application," *Technologies*, vol. 6, no. 2, 2018, Art. no. 44.
- [22] G. D. Clifford et al., "Non-invasive fetal ECG analysis," *Physiol. Meas.*, vol. 35, no. 8, pp. 1521–1536, 2014.
- [23] D. Gurve and S. Krishnan, "Separation of fetal-ECG from single-channel abdominal ECG using activation scaled non-negative matrix factorization," *IEEE J. Biomed. Health Informat.*, vol. 24, no. 3, pp. 669–680, Mar. 2020.
- [24] A. Hyvärinen, "Fast and robust fixed-point algorithms for independent component analysis," *IEEE Trans. Neural Netw.*, vol. 10, no. 3, pp. 626–634, May 1999.
- [25] P. Comon, "Independent component analysis, a new concept?," *Signal Process.*, vol. 36, no. 3, pp. 287–314, 1994.
- [26] R. Plonsey, "Bioelectric phenomena," *Wiley Encyclopedia of Electrical and Electronics Engineering*, 2001.
- [27] B. He and D. Wu, "Imaging and visualization of 3-D cardiac electric activity," *IEEE Trans. Inf. Technol. Biomed.*, vol. 5, no. 3, pp. 181–186, Sep. 2001.
- [28] T. Oostendorp, A. Van Oosterom, and H. Jongsma, "The effect of changes in the conductive medium on the fetal ECG throughout gestation," *Clin. Phys. Physiol. Meas.*, vol. 10, no. 4B, 1989, Art. no. 11.
- [29] Y. Li et al., "Underdetermined blind source separation based on sparse representation," *IEEE Trans. Signal Process.*, vol. 54, no. 2, pp. 423–437, Feb. 2006.
- [30] R. Vullings et al., "A robust physiology-based source separation method for QRS detection in low amplitude fetal ECG recordings," *Physiol. Meas.*, vol. 31, no. 7, pp. 935–951, 2010.
- [31] Y. Jonmohamadi et al., "Source-space ICA for EEG source separation, localization, and time-course reconstruction," *NeuroImage*, vol. 101, pp. 720–737, 2014.
- [32] M. B. Pontifex et al., "Variability of ICA decomposition may impact EEG signals when used to remove eyeblink artifacts," *Psychophysiology*, vol. 54, no. 3, pp. 386–398, 2017.
- [33] F. Andreotti et al., "Robust fetal ECG extraction and detection from abdominal leads," *Physiol. Meas.*, vol. 35, no. 8, pp. 1551–1567, 2014.
- [34] J. A. Behar et al., "Noninvasive fetal electrocardiography for the detection of fetal arrhythmias," *Prenatal Diagnosis*, vol. 39, no. 3, pp. 178–187, 2019.
- [35] R. Sameni and G. D. Clifford, "A review of fetal ECG signal processing: issues and promising directions," *Open Pacing, Electrophysiol. Ther. J.*, vol. 3, pp. 4–20, 2010.
- [36] F. Andreotti et al., "An open-source framework for stress-testing non-invasive foetal ECG extraction algorithms," *Physiol. Meas.*, vol. 37, no. 5, pp. 627–648, 2016.
- [37] M. J. Rooijackers et al., "Low-complexity r-peak detection for ambulatory fetal monitoring," *Physiol. Meas.*, vol. 33, no. 7, pp. 1135–1150, 2012.
- [38] Association for the Advancement of Medical Instrumentation, "American national standard for ambulatory electrocardiographs," ANSI, AAMI EC38-1994, 1994.
- [39] M. A. Stephens, "EDF statistics for goodness of fit and some comparisons," *J. Amer. Stat. Assoc.*, vol. 69, no. 347, pp. 730–737, 1974.
- [40] D. George and P. Mallery, "Descriptive statistics," in *IBM SPSS Statistics 25 Step by Step*, Evanston, IL, USA: Routledge, 2018, pp. 126–134.
- [41] N. Vapnik Vladimir, *The Nature of Statistical Learning Theory*. Berlin, Germany: Springer, 1995.
- [42] G. F. Smits and E. M. Jordaana, "Improved SVM regression using mixtures of kernels," in *Proc. Int. Joint Conf. Neural Netw. (Cat. No 02CH37290)*, 2002, vol. 3, pp. 2785–2790.